International Journal of Heat and Mass Transfer 51 (2008) 5811–5822

Contents lists available at ScienceDirect

International Journal of Heat and Mass Transfer

journal homepage: www.elsevier.com/locate/ijhmt

Axial heat conduction effects in the entrance region of parallel plate ducts

A. Haji-Sheikh [a,*], J.V. Beck [b], Donald E. Amos [c,1]

[a] Department of Mechanical and Aerospace Engineering, The University of Texas at Arlington, Arlington, TX 76019-0023, USA
[b] Department of Mechanical Engineering, Michigan State University, East Lansing, MI 48824-1226, USA
[c] Sandia National Laboratories, Albuquerque, NM 87185, USA

ARTICLE INFO

Article history:
Received 21 February 2008
Received in revised form 30 April 2008
Available online 16 July 2008

Keywords:
Heat transfer
Convection
Axial conduction
Duct flow
Thermal entrance
Parallel-plate ducts

ABSTRACT

Exact series solutions for the computation of temperature in parallel plate channels and circular passages are well known. The inclusion of the contribution of axial conduction leads to a set of modified Graetz type problems for these fluid passages. The emphasis of this paper is the study of the asymptotic variations of wall heat flux values adjacent to the thermal entrance location for parallel plate ducts. The acquired results show interesting variations for different values of the Peclet number near the thermal entrance location. This study reports the unique variations of the wall heat flux values near the location where the wall temperature changes as the Peclet number changes.

1. Introduction

Studies of heat transfer to flow in ducts without the effect of axial conduction are widely available in the literature [1–5]. They include flow in ducts with different cross section profiles. A survey of earlier work describing heat transfer to flow passing through ducts is in [1,2]. Basic information concerning the heat transfer within different passages is in [3–5]. Other studies investigate heat transfer through fluid saturated porous passages, when the axial conduction is negligible [6–11].

In the presence of axial conduction, exact series solutions are limited to Graetz type analysis for one-dimensional passages. Inclusion of axial conduction within these passages is available in [12–17]. Details for the series solution of temperature field in parallel plate channels and circular ducts are in Lahjomri and Oubarra [12]; their methodology is further extended to laminar Hartmann flow in the thermal entrance region in [13]. The Graetz type series solution for flow through saturated porous passages is in Minkowycz and Haji-Sheikh [14], for parallel plate channels and circular ducts. The effect of axial conduction for flow in fluid saturated porous passages with walls at uniform temperature are numerically determined and reported in Nield et al. [18] for parallel plate channel and in Nield et al. [19] for circular ducts. A numerical study of the thermal entrance heat transfer in circular pipes with prescribed wall heat flux is in [20].

It is expected that the axial conduction can have a strong effect on the heat transfer to flow through various flow passages near the entrance region. The convergence of the temperature solutions in parallel plate channels show the convergence for the Graetz type series solution is slow when x is very small. Understanding the nature of the wall heat flux phenomenon near the thermal entrance region is emphasized in this paper. Accordingly, this paper uses a methodology in [21] to enhance the capability of existing powerful analytical tools for determination of the effect of the axial thermal conduction at small distances from the thermal leading edge. In the following sections, the classical series solution and asymptotic solution based on the methodology in [21] are presented and their variations are discussed. The results from this study show that, in this fluid passage, the velocity profile has relatively small effect on heat transfer near the thermal entrance location and the transport of energy is primarily due to thermal conduction.

2. The temperature solutions

Consider a classical steady, laminar, and hydrodynamically fully developed flow between two parallel plates $2H$ apart, see Fig. 1. The velocity profile for flow through parallel plate channels is

$$\frac{u}{U}=\frac{3}{2}\left[1-\left(\frac{\hat{y}}{H}\right)^2\right], \tag{1}$$

where U is the average flow velocity.

* Corresponding author. Tel.: +1 817 272 2010; fax: +1 817 272 2952.
E-mail address: haji@uta.edu (A. Haji-Sheikh).
[1] Retired.

0017-9310/$ - see front matter © 2008 Elsevier Ltd. All rights reserved.
doi:10.1016/j.ijheatmasstransfer.2008.04.056

Nomenclature

A	cross section area $2H \times W$ (m^2)
A_m, B_m	constants in temperature solution
c_n	coefficient in Eq. (10)
c_p	specific heat (J/kg K)
D_m	coefficient for bulk temperature
D_h	hydraulic diameter $4A/P = 4H, m$
E_m	coefficient for wall heat flux
h	heat transfer coefficient in Eq. (15), (W/m^2 K)
h_0	heat transfer coefficient in Eq. (13) (W/m^2 K)
H	parallel plate channel dimension
k	thermal conductivity (W/m K)
m, n	indices
N	selected number of terms in series
Nu_0	$h_0 H/k$, see Eq. (13)
Nu_D	hD_h/k
Pe	Peclet number, UH/α
Pr	Prandtl number $\mu c_p/k$
q_w	local wall heat flux (W/m^2)
Q	total heat flux from a wall (W)
Q^*	dimensionless heat flux from a wall, Eq. (21)
T_i	wall temperature when $x < 0$ (K)
T_b	bulk or mean temperature (K)
T_w	wall temperature when $x > 0$ (K)
u	velocity (m/s)
U	average velocity (m/s)
x	$\hat{x}/H$
$\hat{x}$	axial coordinate (m)
$\bar{x}$	$(\hat{x}/H)/Pe$
y	$\hat{y}/H$
$\hat{y}, \hat{z}$	coordinates normal to $\hat{x}$ in Fig. 1 (m)
Y_1, Y_2	eigenfunctions, $x < 0$, $x > 0$
W	fluid width in $\hat{z}$-direction

Greek symbols

α	thermal diffusivity (m^2/s)
β, β_m	eigenvalues when $x < 0$
Γ	perimeter $W + W$ (m)
λ, λ_m	eigenvalues when $x > 0$
θ	dimensionless temperature
ρ	density (kg/m^3)

Subscripts

1, 2	$x < 0$ or $x > 0$
b	bulk temperature
c	by conduction
L	large x
S	small x

Superscripts

−, +	$x < 0$ or $x > 0$

In the absence of frictional heating and temperature dependence of the thermal conductivity, the temperature distribution obtainable from the energy equation is

$$u\frac{\partial T}{\partial \hat{x}} = \frac{k}{\rho c_p}\left(\frac{\partial^2 T}{\partial \hat{x}^2} + \frac{\partial^2 T}{\partial \hat{y}^2}\right). \tag{2}$$

Introduce the Peclet number $Pe = \rho c_p HU/k$ and the dimensionless coordinates $x = \hat{x}/H$, $y = \hat{y}/H$, and $\bar{x} = x/Pe$ into this equation; then Eq. (2) becomes:

$$\frac{\partial^2 T}{\partial y^2} = \frac{u}{U}\frac{\partial T}{\partial \bar{x}} - \frac{1}{Pe^2}\frac{\partial^2 T}{\partial \bar{x}^2}. \tag{3}$$

The wall temperature, as depicted in Fig. 1, is the constant T_i when $x < 0$ and it is the constant T_w, when $x > 0$. For convenience in mathematical formulation the dimensionless temperature is designated as $\theta_1 = (T - T_i)/(T_i - T_w)$, when $x < 0$ and $\theta_2 = (T - T_w)/(T_i - T_w)$, when $x > 0$. Using these dimensionless temperature functions, the governing partial differential equation, Eq. (3), for these two regions takes the following forms

$$\frac{\partial^2 \theta_i}{\partial y^2} = \frac{u}{U}\frac{\partial \theta_i}{\partial \bar{x}} - \frac{1}{Pe^2}\frac{\partial^2 \theta_i}{\partial \bar{x}^2}$$
$$\text{with } \frac{\partial \theta_i}{\partial y} = 0 \text{ at } y = 0 \text{ and } \theta_i = 0 \text{ at } y = 1 \tag{4}$$

for $i = 1$ or 2. Other conditions are $\theta_1(-\infty, y) = 0$ and $\theta_2(\infty, y) =$ finite while the compatibility conditions are $(\partial\theta_2/\partial\bar{x})_{\bar{x}=0} = (\partial\theta_1/\partial\bar{x})_{\bar{x}=0}$ and $\theta_2(0, y) - \theta_1(0, y) = 1$.

The emphasis of this study is to predict heat transfer rate for all x values between 0 and ∞. For larger values of x, the solution for each θ_i in Eq. (4) with the specified boundary condition is sought. The mathematical formulation of these solutions at large values of x is readily available in the literature [12,14]. However, because of minor differences, a brief description of the solution is in the next section. The following sections also include the asymptotic solutions at very small x values.

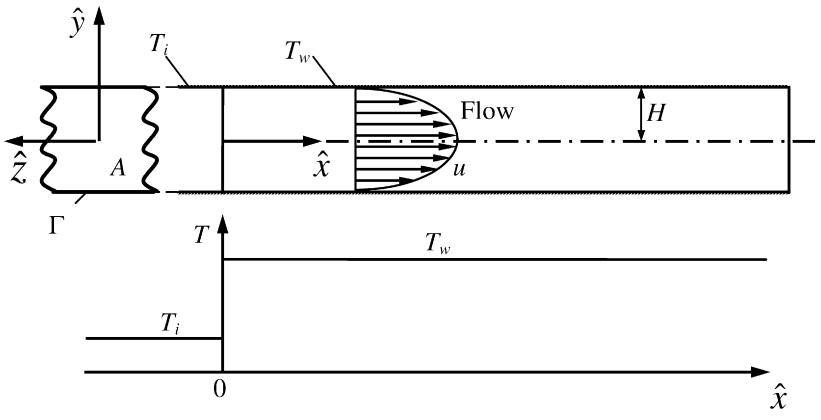

Fig. 1. Schematic of a parallel plate channel with temperature change at $\hat{x} = 0$.

2.1. Extended graetz solution

The solution of the partial differential equation, Eq. (4), is obtainable using the method of separation of variables by setting $\theta_i(\bar{x},y) = X(\bar{x})Y(y)$ for $i = 1$ or 2. The substitution of this functional form for θ_i in Eq. (4) yields:

$$\frac{Y''}{Y} = \frac{u}{U}\frac{X'}{X} - \frac{1}{Pe^2}\frac{X''}{X}. \tag{5a}$$

Although $u = u(y)$ is present on the right side of Eq. (5a), it is possible to separate the variables. Let X be defined by equation:

$$X'(\bar{x}) = \beta^2 X(\bar{x}), \tag{5b}$$

and, following differentiation and appropriate substitution, to get $X''(\bar{x}) = \beta^2 X'(\bar{x}) = \beta^4 X(\bar{x})$. This leads to the following differential equation for computation of $Y(y)$:

$$Y''(y) - \beta^2\left(\frac{u}{U}\right)Y(y) + \frac{\beta^4}{Pe^2}Y(y) = 0, \tag{6}$$

where the parameter β in Eq. (6) is the eigenvalue. Since the solution for $X(\bar{x})$ in Eq. (5b) is $\exp(\beta^2\bar{x})$ multiplied by a constant, this methodology leads to the following temperature solutions for θ_1 and θ_2:

$$\theta_i(\bar{x},y) = \begin{cases} \sum_{m=1}^{\infty} A_m e^{\beta_m^2\bar{x}} Y_{i,m}(y), & \text{for } i = 1 \\ \sum_{m=1}^{\infty} B_m e^{\beta_m^2\bar{x}} Y_{i,m}(y), & \text{for } i = 2 \end{cases}. \tag{7}$$

In this equation $\theta_1(\bar{x},y)$ is finite and goes to zero as $\bar{x} \to -\infty$ and $\theta_2(\bar{x},y)$ is also finite and goes to zero as $\bar{x} \to +\infty$. Therefore, when $\bar{x} < 0$, the eigenvalue β_m is real; however, when $\bar{x} > 0$, the coefficient β_m for inclusion in Eq. (7) becomes imaginary. The compatibility conditions at $\bar{x} = 0$ provided the coefficients A_m and B_m as they appear in Appendix A. This leads to the following forms for $\theta_1(\bar{x},y)$ and $\theta_2(\bar{x},y)$:

$$\theta_1(\bar{x},y) = \sum_{m=1}^{\infty} A_m Y_{1,m}(y) e^{-\beta_m^2|\bar{x}|} \quad \text{when } x < 0, \tag{8a}$$

and by selecting $\beta = i\lambda$ in Eqs. (5b) and (6) to get

$$\theta_2(\bar{x},y) = \sum_{m=1}^{\infty} B_m Y_{2,m}(y) e^{-\lambda_m^2\bar{x}} \quad \text{when } x > 0. \tag{8b}$$

Therefore, both β_m and λ_m, in Eqs. (8a,b), for the $\theta_1(\bar{x},y)$ and $\theta_2(\bar{x},y)$ solutions are positive and real.

Because the computation of $\theta_2(\bar{x},y)$ is the primary objective in heat transfer applications, Eq. (6) is initially utilized after replacing β with $i\lambda$. Once the value of u/U from Eq. (1) is placed in the modified form of Eq. (6), it becomes:

$$Y''(y) + \frac{3}{2}\lambda^2[1-(y)^2]Y(y) + \frac{\lambda^4}{Pe^2}Y(y) = 0, \tag{9}$$

with boundary conditions $Y'(y)$=0 at $y = 0$ and $Y(y) = 0$ at $y = 1$. The solution of this differential equation has a hypergeometric power series form

$$Y(y) = \sum_{n=0}^{\infty} c_n y^n, \tag{10}$$

wherein $y = \hat{y}/H$. After substituting $Y(y)$ from Eq. (10) in Eq. (9), the result is

$$\sum_{n=2}^{\infty} c_n n(n-1)y^{n-2} + \frac{3}{2}\lambda^2(1-y^2)\sum_{n=0}^{\infty} c_n y^n + \left(\lambda^4/Pe^2\right)\sum_{n=0}^{\infty} c_n y^n = 0. \tag{11}$$

The term that includes y^0 suggests c_0 = constant = 1. Because of symmetry in y-direction, the parameter n is an even integer. When $n > 1$, the other constants are obtainable from the relations:

$$c_2 = -\frac{1}{2}[\lambda^4/Pe^2 + (3/2)\lambda^2], \tag{12a}$$

$$c_{n+2} = -\frac{(\lambda^4/Pe^2)c_n + (3/2)\lambda^2(c_n - c_{n-2})}{(n+2)(n+1)}. \tag{12b}$$

Substitution of these c_n coefficients in Eq. (10) produces the eigenfunction $Y_2(y)$ to be used for determination of $\theta_2(\bar{x},y)$ in Eq. (8b). After replacing λ^2 with $-\beta^2$, Eqs. (12a,b) provide a new set of c_n coefficients; Eq. (10) produces the eigenfunction $Y_1(y)$ for determination of $\theta_1(\bar{x},y)$ in Eq. (8a). For either region, it becomes necessary to simultaneously determine the coefficients c_n and the eigenvalues β_m^2 and λ_m^2 for $m = 1,2,\ldots$. This requires the inclusion of the eigencondition $Y_i(1) = 0$ to be used for finding these eigenvalues.

Once the functional forms of $Y_i(y)$ are in hand, the thermal compatibility conditions at $\bar{x} = 0$ location $\theta_2(0,y) - \theta_1(0,y) = 1$ and $\partial\theta_1/\partial\bar{x}|_{\bar{x}=0} = \partial\theta_2/\partial\bar{x}|_{\bar{x}=0}$ provide A_m and B_m parameters. The method of determination of A_m and B_m using these compatibility conditions is combined with that for circular pipes in [12]. Summaries of the orthogonality conditions for determination of A_m and B_m for parallel plate ducts and other related quantities are in the Appendix A.

2.2. The small-x solution

At very small x values, the existing solutions of Eq. (2) are in the infinite series form. Convergences of these series become very difficult when x is very small. It is shown in [21] that, for flow over a flat plate, the two limiting solutions for slug flow and no flow converge near the thermal entrance location. Therefore, a no flow condition serves as the lower limit and a slug flow condition serves as the upper limit. It is expected that the actual solution would fall between these two solutions. These two limiting solutions, as presented in [21], are utilized in the subsequent formulations. The dimensionless quantity to be used is the special Nusselt number:

$$Nu_0 = \frac{h_0 H}{k}, \tag{13}$$

where $h_0 = q_w/(T_w - T_i)$.

To demonstrate the special feature of h_0, the computed Nu_0 data from the series solution, using Eqs. (8b) and (A.4), are plotted in Fig. 2. Different symbols indicate the pre-selected number of eigenvalues N as presented in the figure; they show the convergence of $Nu_0(x)$ for $Pe = 1$ as N increases in the θ_2 solution. It is desirable to compare these series solutions with that for a slug flow over a flat plate [21], wherein the slug flow and no flow solutions converge to the same values at very small $\hat{x}$. The solid line in Fig. 2 shows this expected upper limit for Nu_0 taken from [21], Eq. (23b), since $St = Nu_0/Pe$, as

$$Nu_0 = \frac{Pe}{2\pi}\exp(xPe/2)[K_0(xPe/2) + K_1(xPe/2)], \tag{14}$$

where $K_0(xPe/2)$ and $K_1(xPe/2)$ are the modified Bessel functions. This equation approaches the dash line for the no flow condition when x is very small. It is remarkable that, at small x, the series solution data clearly approach the dash line for $Nu_0 = 1/(\pi x)$, taken from [21], Eq. (16) for the no flow condition. Therefore, Eq. (14) asymptotically approaches $Nu_0 \cong 1/(\pi x)$ as x becomes very small. Since this lower limit is for no flow condition, it implies that at small x values, the data for other Peclet numbers should behave similarly. To show this unique behavior, the data for $Pe = 2$, 5, and 10 are plotted in Fig. 3 in addition to those for $Pe = 1$. Indeed, the data in Fig. 3 for the $Pe = 2$, 5, and 10, show similar behaviors as those for $Pe = 1$. For comparison, the solid lines represent Eq. (14)

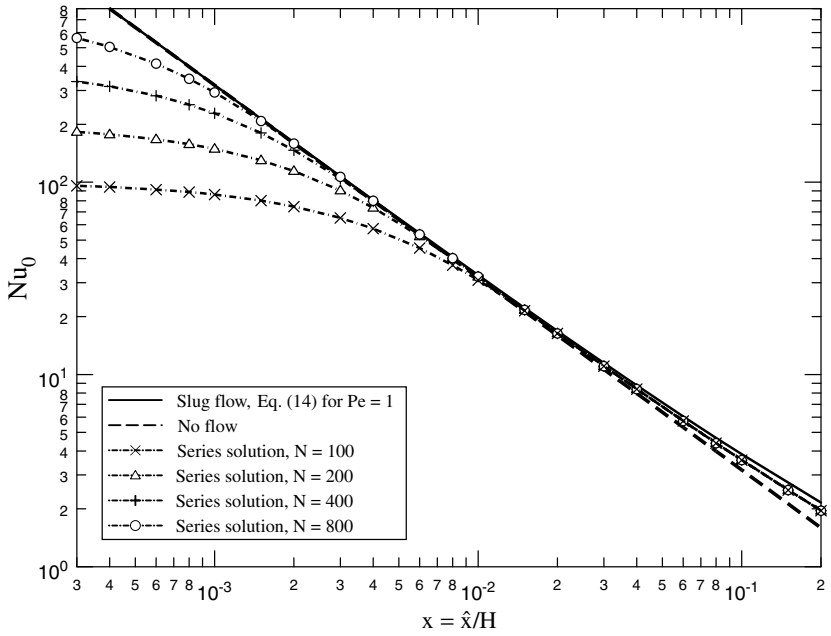

Fig. 2. The limiting Nusselt number Nu_0 at small $x = \hat{x}/H$-values for laminar flow in parallel plate channels when $Pe = 1$.

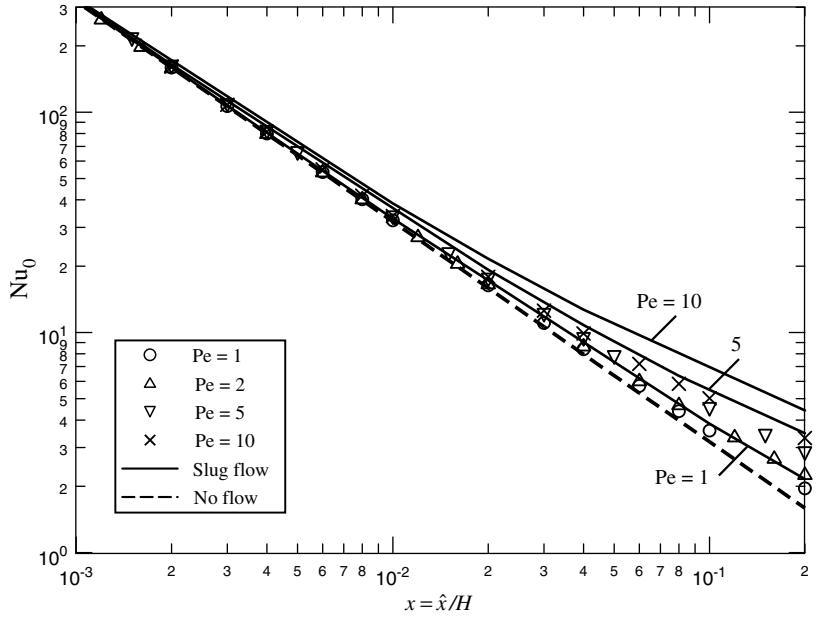

Fig. 3. The Nusselt number Nu_0 at small $x = \hat{x}/H$-values for laminar flow in parallel plate channels.

for $Pe = 1$, 5, and 10. Moreover, when $x < 0$, the dash line in Fig. 3 serves as an upper limit for Nu_0 when x is very small x.

3. Results and discussion

The definition of Nu_0 presented in earlier sections uses the heat transfer coefficient $h_0 = q_w/(T_w - T_i)$, where both q_w and h_0 are positive when $T_w > T_i$. This is different from the standard definition of the heat transfer coefficient; e.g., when $\bar{x} > 0$, $h = q_w/(T_w - T_b)$, where T_b is the bulk or mean temperature. Then, the commonly used heat transfer coefficient h is related to the earlier defined h_0 by the relation:

$$h = \left(\frac{h_0}{\theta_b}\right). \tag{15}$$

To demonstrate the variation of the bulk temperature $\theta_b = (T_b - T_w)/(T_i - T_w)$, samples of computed data are presented in Column 6 of Table 1, where $\theta_b(\bar{x}) = \theta_{2,b}(\bar{x})$, see Eq. (A.5). Fig. 4 shows that the variations of $\theta_b(\bar{x})$ as a function of the axial coordinate $\bar{x}$ for different values of Pe, when $\bar{x} > 0$. Also, the solid lines in Fig. 4 indicate that the slopes of θ_b lines are small at very small values of $\bar{x}$. The dot-dash line in this figure represents the θ_b values in the absence of axial conduction.

As discussed in [21], thermal conduction dominates when x is very small. The study in [21] is validated for flow in parallel plate ducts by the data presented in Figs. 2 and 3 as they show that thermal conduction near the entrance region dominates. Indeed, as is demonstrated in [21], both the no flow solution and the slug flow solution produce $Nu_0 = 1/(\pi x)$ with $x = \hat{x}/H$ near the thermal entrance location. The utilization of this concept enables the determi-

Table 1a
Selected values of $Nu_0 = h_0H/k$, $Nu_H = hH/k$, Q^*, and θ_b for heat transfer in parallel plate ducts when $Pe = 1$ and 2

Pe	$\bar{x} = \frac{x}{Pe}$	$\frac{h_0H}{k}$	$\frac{hH}{k}$	Q^*	θ_b
1	0.004	80.012	119.97	2.4627	0.6669
	0.006	53.489	80.385	2.3328	0.6654
	0.008	40.225	60.590	2.2404	0.6639
	0.01	32.267	48.713	2.1685	0.6624
	0.02	16.347	24.961	1.9435	0.6549
	0.04	8.3817	13.091	1.7143	0.6403
	0.06	5.7214	9.1391	1.5768	0.6260
	0.08	4.3876	7.1668	1.4770	0.6122
	0.10	3.5844	5.9865	1.3979	0.5987
	0.2	1.9574	3.6489	1.1389	0.5364
	0.4	1.0967	2.5364	0.8517	0.4324
	0.6	0.7729	2.2110	0.6684	0.3496
	0.8	0.5877	2.0765	0.5337	0.2830
	1.0	0.4617	2.0133	0.4295	0.2293
	2	0.1567	1.9503	0.1494	0.0803
	4	0.0192	1.9477	0.0184	0.0099
	6	2.37 E−3	1.9477	2.26 E−3	1.22 E−3
2	0.001	158.89	201.86	1.7513	0.7871
	0.002	80.351	102.72	1.6403	0.7822
	0.004	40.564	52.044	1.5285	0.7794
	0.006	27.299	35.144	1.4624	0.7768
	0.008	20.665	26.694	1.4151	0.7742
	0.01	16.684	21.624	1.3780	0.7715
	0.02	8.7153	11.487	1.2601	0.7587
	0.04	4.7159	6.4241	1.1348	0.7341
	0.06	3.3702	4.7426	1.0557	0.7106
	0.08	2.6886	3.9067	0.9958	0.6882
	0.1	2.2730	3.4092	0.9464	0.6667
	0.2	1.3967	2.4457	0.7721	0.5711
	0.4	0.8616	2.0374	0.5557	0.4229
	0.6	0.6131	1.9494	0.4104	0.3145
	0.8	0.4509	1.9255	0.3049	0.2342
	1	0.3346	1.9186	0.2270	0.1744
	2	0.0766	1.9157	0.0521	0.0400
	4	4.03×10^{-3}	1.9157	2.74×10^{-3}	2.11×10^{-3}

Table 1b
Selected values of $Nu_0 = h_0H/k$, $Nu_H = hH/k$, Q^*, and θ_b for heat transfer in parallel plate ducts when $Pe = 5$ and 10

Pe	$\bar{x} = \frac{x}{Pe}$	$\frac{h_0H}{k}$	$\frac{hH}{k}$	Q^*	θ_b
5	0.001	65.043	71.569	1.2026	0.9088
	0.002	33.207	36.631	1.1571	0.9065
	0.004	17.281	19.158	1.1103	0.9020
	0.006	11.966	13.331	1.0817	0.8976
	0.008	9.3037	10.415	1.0607	0.8933
	0.01	7.7029	8.6647	1.0438	0.8890
	0.02	4.4773	5.1553	0.9866	0.8685
	0.04	2.8148	3.3876	0.9173	0.8309
	0.06	2.2258	2.7935	0.8676	0.7968
	0.08	1.9106	2.4967	0.8265	0.7653
	0.1	1.7075	2.3206	0.7905	0.7358
	0.2	1.2184	1.9969	0.6483	0.6101
	0.4	0.8086	1.9011	0.4504	0.4253
	0.6	0.5630	1.8931	0.3148	0.2974
	0.8	0.3936	1.8924	0.2201	0.2080
	1	0.2753	1.8923	0.1540	0.1455
	2	0.0461	1.8923	0.0258	0.0243
10	0.0004	81.572	85.375	1.0964	0.9555
	0.0006	55.046	57.653	1.0831	0.9548
	0.0008	41.779	43.788	1.0735	0.9541
	0.001	33.817	35.467	1.0660	0.9535
	0.002	17.882	18.818	1.0420	0.9503
	0.004	9.8892	10.474	1.0160	0.9442
	0.006	7.2040	7.6781	0.9993	0.9382
	0.008	5.8475	6.2705	0.9863	0.9325
	0.01	5.0235	5.4191	0.9755	0.9270
	0.02	3.3142	3.6764	0.9357	0.9015
	0.04	2.3525	2.7431	0.8809	0.8576
	0.06	1.9709	2.4049	0.8381	0.8195
	0.08	1.7495	2.2280	0.8011	0.7852
	0.1	1.5982	2.1207	0.7677	0.7536
	0.2	1.1981	1.9296	0.6307	0.6209
	0.4	0.8072	1.8887	0.4339	0.4274
	0.6	0.5561	1.8872	0.2991	0.2947
	0.8	0.3834	1.8871	0.2063	0.2032
	1	0.2644	1.8871	0.1422	0.1401
	2	0.0412	1.8871	0.0222	0.0218

nation of Nu_D for small x values following the determination of $\theta_b(0)$ and utilization of Eq. (15). Then, the asymptotic values Nu_D are obtained from the methodology presented in [21] for $x > 0$, from equation:

$$Nu_{D,S} = \left(\frac{D_h}{H}\right)\left(\frac{1}{\theta_b(0)}\right)\left(\frac{1}{\pi Pe\bar{x}}\right). \tag{16}$$

Using $\bar{x} = x/Pe$, $Nu_{D,S}$ is plotted as dash lines in Fig. 5 for $Pe = 1, 2, 5$, and 10. Also, Fig. 5 shows the series solution for $Nu_D = 4Nu_H$ as a function of $\bar{x} = (\hat{x}/H)/Pe$ for the same Peclet numbers, using (A.6). A sample of the plotted data is readily available since $Nu_D = 4(hH/k)$ and the values of hH/k are in the Column 4 of Table 1 for these Pe values. There is a remarkable agreement between these two sets of data, at small x values, that attest to the validity of the finding reported in [21].

Also, it is possible to estimate the values of $\theta_b(0)$ for other Pe values from the new empirical Eq. (B.1) in Appendix B:

$$\theta_b(0) = \frac{0.95 + Pe^{4/3}}{1.90 + Pe^{4/3}}, \tag{17}$$

which predicts the exact $\theta_b(0)$ values with a reasonable accuracy. This equation satisfies the limiting conditions: $\theta_b(0) = 1$, when $Pe = \infty$ and $\theta_b(0) = 1/2$ when $Pe = 0$ and yields $\theta_b(0)$ values with an error of less than 0.45% for $Pe \geqslant 1$. The computed values of $\theta_b(0)$ for different values of Pe are in Tables 2a,b. It is to be noted that $\theta_b(0)$ in Table 2b are the same as those in Table 2a although the eigenvalues and other related parameters are different. Then, after placing $\theta_b(0)$ from Eq. (17) in Eq. (16), the small x asymptotic solution for Nu_D becomes:

$$Nu_{D,S} = \frac{4(1.90 + Pe^{4/3})}{\pi Pe(0.95 + Pe^{4/3})}\left(\frac{1}{\bar{x}}\right). \tag{18}$$

The dashed lines in Fig. 5 are from this asymptotic solution, Eq. (18). There is a remarkable agreement between these empirical data and those obtained from the series solutions near the entrance location. Also, Fig. 5 includes the classical variation of Nu_D as a function of $\bar{x} = x/Pe$ in the absence of axial conduction [22]. For $Pe \leqslant 10$, the data in Fig. 5 show rather large errors in the Nu_D values in the thermal entrance region when axial conduction is neglected and the dash lines in Fig. 5 make Eq. (18) a valuable tool for the estimation of error if the axial thermal conduction is neglected. When $\bar{x}$ is very large $Nu_D = 7.791$ for $Pe = 1$ which is slightly larger than 7.541 for no axial conduction case. The other Nu_D values are in Table 2.

3.1. Approximate solutions for bulk temperature

The availability of approximate solutions for the bulk temperature and heat transfer coefficient is desirable in various engineering applications. Information of this type is useful in the design of heat exchangers and other similar devices.

Knowledge of the bulk temperature facilitates predicting the energy transferred to the moving fluid. For convenience of this presentation, a single definition for the bulk temperature, $\theta_b = (T_b - T_w)/(T_i - T_w)$, is selected for the entire domain. Consider first the bulk temperature, for $\bar{x} < 0$. The definition of bulk temperature is

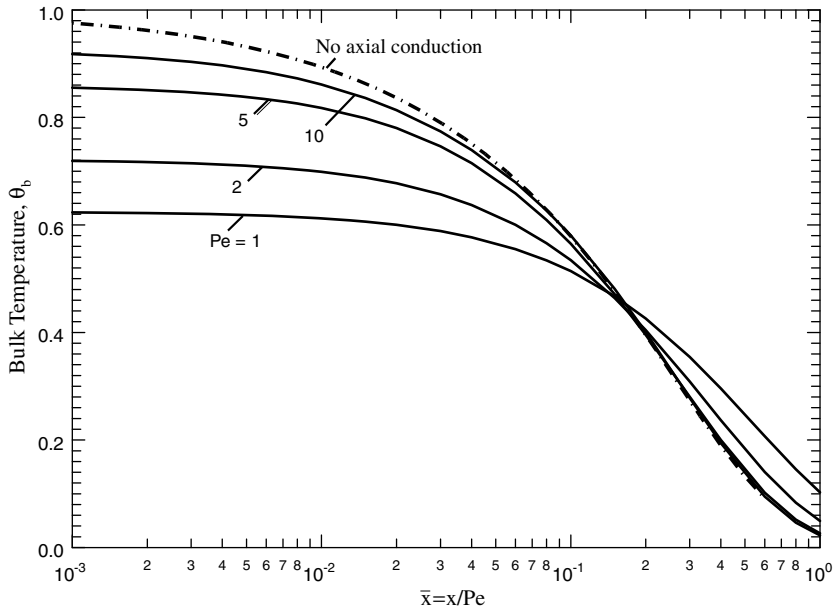

Fig. 4. Bulk temperature as a function of $\bar{x} = (\hat{x}/H)/Pe$ and the Peclet number, for parallel plate channels.

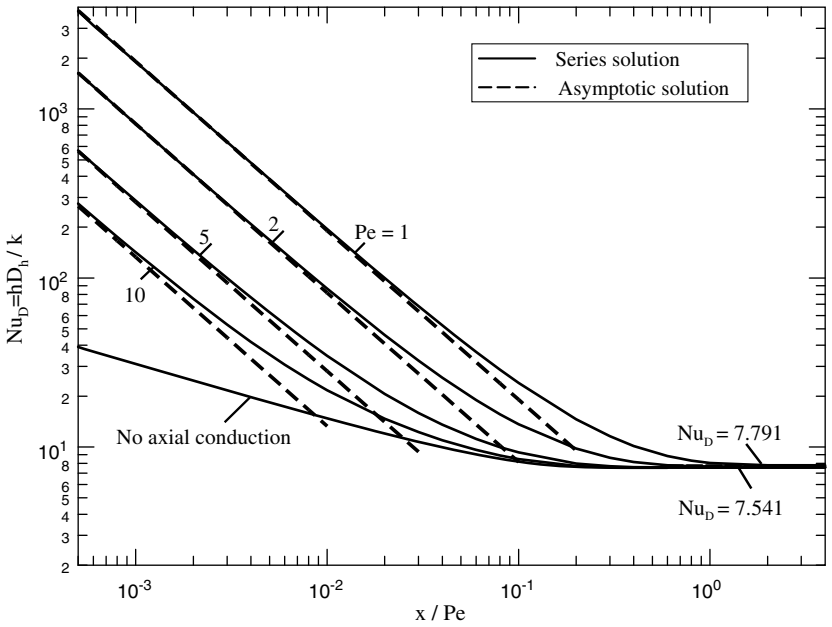

Fig. 5. Variation of Nu_D and its asymptotic solution for parallel plate channels as a function of $\bar{x} = (\hat{x}/H)/Pe$ and the Peclet number.

$$\theta_b = \int_0^1 \left(\frac{u(y)}{U}\right)\left(\frac{T - T_w}{T_i - T_w}\right) dy. \tag{19a}$$

Now, replace $(T - T_w)/(T_i - T_w)$ by $1 + \theta_1(\bar{x}, y)$ and use Eq. (8a) to get $\theta_b(\bar{x}) = 1 + \theta_{1,b}(\bar{x})$ or

$$\theta_b = 1 + \sum_{m=1}^{\infty} A_m \left[\int_0^1 \left(\frac{u(y)}{U}\right) Y_{1,m}(y)\, dy\right] e^{-\beta_m^2 |\bar{x}|}$$

$$= 1 + \sum_{m=1}^{\infty} D_m^- e^{-\beta_m^2 |\bar{x}|}, \tag{19b}$$

with $u(y)/U$ from Eq. (1). Consider next $\bar{x} > 0$, replacing $(T - T_w)/(T_i - T_w)$ in Eq. (19a) by $\theta_2(\bar{x}, y)$ from Eq. (8b) yields $\theta_b(\bar{x}) = \theta_{2,b}(\bar{x})$ or

$$\theta_b = \sum_{m=1}^{\infty} B_m \left[\int_0^1 \left(\frac{u(y)}{U}\right) Y_{2,m}(y)\, dy\right] e^{-\lambda_m^2 \bar{x}} = \sum_{m=1}^{\infty} D_m^+ e^{-\lambda_m^2 \bar{x}}. \tag{19c}$$

When $\bar{x}$ is relatively large and $\bar{x} > 0$, the only needed eigenvalue is λ_1; computed parameters D_1^+ and λ_1^2 are in given Table 1b for different Pe numbers. Then, one can set $\theta_{b,L}(x) \cong D_1^+ \exp(-\lambda_1^2 x/Pe)$ when x is large and set $\theta_{b,S}(x) = \theta_b(0) \exp(-\lambda_1^2 x/Pe)$ when x is small. A linear interpolation between $\theta_{b,S}(x)$ and $\theta_{b,L}(x)$ leads to a useful and valuable relation:

$$\theta_b(x) = \left[\frac{x\theta_{b,L}(x) + 0.25\theta_{b,S}(x)}{x + 0.25}\right]$$

$$= \left[\frac{xD_1 + 0.25\theta_b(0)}{x + 0.25}\right] \exp(-\lambda_1^2 x/Pe), \tag{20a}$$

for heat exchanger design applications. Values computed using this equation are plotted in Fig. 6a and are compared with those appearing in Table 1. The results show good accuracy for this method of

Table 2a
First eigenvalue, first constant E_1^+ for Nu_0, and first constant D_1^+ for θ_b, $\theta_b(0)$, and $Nu_D(\infty)$ for different Pe values, when $x > 0$

Pe	λ_1^2	D_1^+	E_1^+	$\theta_b(0)$	$Nu_D(\infty)$
0.00	0.0	0.49277	1.0	0.5	8.1174
0.01	0.015643	0.49450	1.00290	0.50184	8.1124
0.05	0.076927	0.50144	1.01453	0.50918	8.0929
0.1	0.15069	0.51011	1.02908	0.51835	8.0695
0.2	0.28915	0.52737	1.05814	0.53662	8.0258
0.5	0.63897	0.57785	1.14363	0.58997	7.9165
1	1.04790	0.65338	1.27260	0.66998	7.7909
2	1.47231	0.76025	1.45644	0.78472	7.6629
3	1.65374	0.81902	1.55796	0.85017	7.6089
5	1.78783	0.86934	1.64508	0.91109	7.5693
7	1.83297	0.88785	1.67715	0.93744	7.5560
10	1.85887	0.89886	1.69624	0.95673	7.5484
20	1.87846	0.90739	1.71103	0.97866	7.5426
30	1.88218	0.90903	1.71387	0.98585	7.5415
50	1.88409	0.90987	1.71534	0.99155	7.5410
70	1.88462	0.91011	1.71575	0.99398	7.5408
100	1.88490	0.91023	1.71597	0.99579	7.5408
∞	1.88518	0.91035	1.71617	1.00000	7.5407

Table 2b
First eigenvalue, first constant $|E_1^-|$ for Nu_0, and first constant $|D_1^-|$ for θ_b, $\theta_b(0)$, and $Nu_D(\infty)$ for different Pe values, when $x < 0$

Pe	β_1^2/Pe	$\lvert D_1^-\rvert$	$\lvert E_1^-\rvert$	$\theta_b\,(0)$	$Nu_D(-\infty)$
0.00	$\pi/2$	$48/\pi^4$	1	1/2	$\pi^4/12$
0.01	1.57733	0.49103	0.99710	0.50184	8.122
0.05	1.60373	0.48410	0.98551	0.50918	8.143
0.1	1.63732	0.47545	0.97108	0.51835	8.170
0.2	1.70649	0.45824	0.94250	0.53662	8.227
0.5	1.92947	0.40817	0.86040	0.58997	8.432
1	2.34822	0.33408	0.74389	0.66998	8.907
2	3.31342	0.23289	0.61562	0.78472	10.573
3	4.35107	0.18272	0.62690	0.85017	13.723
5	6.27106	0.14095	0.97378	0.91109	27.635
7	7.75776	0.10601	1.37697	0.93744	51.954
10	9.50957	0.07263	1.78668	0.95673	98.399
20	13.8495	0.03528	2.72211	0.97866	308.59
30	17.1592	0.02332	3.42434	0.98585	587.34
50	22.3954	0.01389	4.52970	0.99155	1304.4

estimation, with error of ~1% or less. In the absence of tabulated data, relations for quick estimation of D_1^+ and λ_1^2 are in Appendix B. A modified form of Eq. (20a) for determination of $\theta_b(|x|) = 1 + \theta_{1b}(|x|)$, when $x < 0$, is

$$\theta_b(|x|) = \left[\frac{|x|\theta_{b,L}(|x|) + 0.25\theta_{b,S}(|x|)}{|x| + 0.25}\right], \tag{20b}$$

where $\theta_{b,L}([x]) = 1 - |D_1^-|\exp(-\beta_1^2|x|/Pe)$ and $\theta_{b,S}([x]) = 1 - [1 - \theta_b(0)]\exp(-\beta_1^2|x|/Pe)$. The subscripts L and S stand for large and small values of x. As in the previous case, the numerical values for $\theta_b(|x|)$ acquired using Eq. (20b) are plotted in Fig. 6b and compared with the solid lines for the exact series solution. The results in this figure show excellent agreement. Indeed, when $x < 0$, both $\theta_{b,S}(|x|)$ and $\theta_{b,L}(|x|)$ can estimate $\theta_b(|x|)$ over a relatively large range of x.

For estimation of the Nusselt number $Nu_{0,L} = E_1^+\exp(-\lambda_1^2 x/Pe)$ at large $x > 0$, the parameter E_1^+ is in Table 1b for different Pe values. An approximate relation for the estimation of E_1^+ is given in the Appendix B. Fig. 7a shows the range of acceptable performance for the parameters E_1^+ and λ_1^2 for determination of $Nu_{0,L}$. Indeed, the asymptotic solution at large x values agrees well with the exact solution within a relatively large range depending on the Peclet number. The dot-dash line for no flow condition, in Fig. 7a, describes the asymptotic function $Nu_{0,S} = 1/(\pi x)$ employed in the formulation of Eq. (18), also plotted in Fig. 7a. Similar solutions are obtained when $x < 0$ and plotted in Fig. 7b. The data for solutions at small $|x|$ behave similar to those in Fig. 7a, except the no flow solution serves as an upper limit.

4. Total wall heat flux

Knowledge of total heat flux from a wall of the duct is needed information in many heat transfer applications. The computation of total wall heat flux near the $x = 0$ location is a critical issue and a related discussion is in [21]. The function $Q^*(\bar{x})$ as it appears in Table 1 is

$$Q^*(\bar{x}) = \int_{\bar{x}}^{\infty} Nu_0(\bar{x})\mathrm{d}\bar{x}, \tag{21}$$

and it is related to the total wall heat flux. When W is a length perpendicular to the $\hat{x}\hat{y}$-plane, the heat flux entering a differential fluid element from a wall is $\mathrm{d}Q(\hat{x}) = h_0(\hat{x})(T_w - T_i)W\mathrm{d}\hat{x}$ and upon integration from $\hat{x}$ to ∞, it becomes

$$\frac{Q/W}{k(T_w - T_i)} = \int_{\hat{x}}^{\infty}\frac{h_0}{k}\mathrm{d}\hat{x} = \int_x^{\infty}\frac{h_0 H}{k}\mathrm{d}x. \tag{22a}$$

The functional form of the heat transfer coefficient obtained from the series solution is $h_0 = h_0(\bar{x})$. For convenience in numerical computation, the axial coordinate x is replaced by $\bar{x}$ and Eq. (22a) is written as

$$\begin{aligned}\frac{Q/W}{k(T_w - T_i)} &= Pe\int_{\bar{x}}^{\infty}\frac{h_0(\bar{x})H}{k}\mathrm{d}\bar{x} = Pe\int_{\bar{x}}^{\infty}Nu_0(\bar{x})\mathrm{d}\bar{x}\\ &= PeQ^*(\bar{x}).\end{aligned} \tag{22b}$$

The function $Q^*(\bar{x})$ data in Table 1 are finite and they approach the $\theta_b(\bar{x})$ data when Pe becomes large. Additionally, an examination of the limiting solution shows that the magnitude of total wall heat flux becomes infinite as x goes to zero. This happens when the continuum condition is no longer exists; a detailed discussion of this issue is in [21]. For this reason, Eq. (22b) provides the magnitude of total wall heat flux between any finite $\bar{x}$ location and ∞. The asymptotic values of dimensionless wall heat flux are the subject of next presentation. The solid lines in Fig. 8a represent the computed values of $Q^*(x/Pe)$ as they appear in Table 1, but plotted versus the axial coordinate x. This procedure is repeated when $x < 0$ and the computed results are in Fig. 8b.

Asymptotic values to $Q^*(x)$ at large x are readily available by retaining the one term solution for $Nu_0(\bar{x})$ (see Eq. (A.4)) and placing it in Eq. (22b) to get

$$Q_L^*(x) = \frac{E_1^+ e^{-\lambda_1^2 x/Pe}}{\lambda_1^2}. \tag{23}$$

Next, applying an energy balance to a volume element with a thickness $\mathrm{d}\hat{x}$, as shown in Fig. 9, leads to the relation:

$$\rho c_p UHW\mathrm{d}T_b + \mathrm{d}Q_c = h_0 W\mathrm{d}\hat{x}(T_w - T_i), \tag{24a}$$

where Q_c represents the contribution of axial conduction in the $\hat{x}$-direction within the cross section of the duct. By definition $\theta_b = (T_b - T_w)/(T_i - T_w)$ and, therefore, in dimensionless space, Eq. (24a) can be written as

$$\frac{h_0 H}{k}\frac{\mathrm{d}x}{Pe} = -\mathrm{d}\theta_b - \frac{1}{Pe}\frac{\mathrm{d}Q_c/W}{k(T_w - T_i)}. \tag{24b}$$

Since $\theta_b(\infty) = Q_c(\infty) = 0$, the integration of the Eq. (24b) between $\bar{x}$ and ∞, after replacing the axial coordinate, yields:

$$Q^*(\bar{x}) = \int_{\bar{x}}^{\infty} Nu_0\mathrm{d}\bar{x} = \theta_b(\bar{x}) + \frac{1}{Pe}\frac{Q_c(\bar{x})/W}{k(T_w - T_i)}. \tag{25}$$

Based on this equation, the contribution of the dimensionless axial conduction:

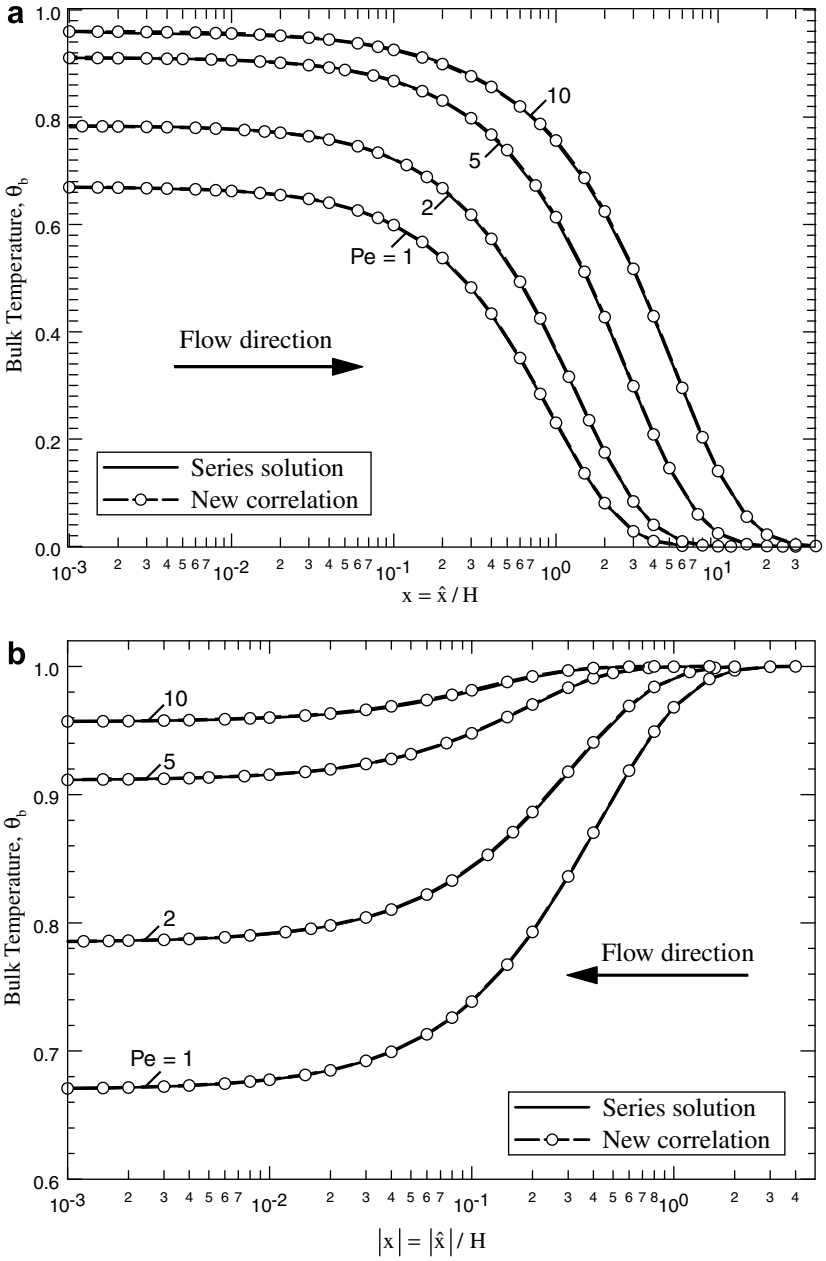

Fig. 6. A comparison of estimated θ_b with those from the series solution: (a) when $x > 0$; and (b) when $x < 0$.

$$\frac{Q_c(\bar{x})/W}{k(T_w - T_i)},$$

is the difference between the entries within the last two columns of Table 1, multiplied by *Pe*. An examination of data at small *x* values in Figs. 3 and 8 leads to a relation for the estimation of the axial conduction at very small *x* values from Eq. (16) in [21]; that is $-\ln(x)/(\pi Pe)$ using the axial coordinate *x*. This makes $Q_S^*(x) = \theta_b(x) - \ln(x)/(\pi Pe)$ with an error of ±3% when $x < 0.01$. Inserting a correction factor in this $Q_S^*(x)$ function reduces error and produces

$$Q_S^*(x) = \theta_{b,S}(x) - \frac{\ln(x)}{\pi Pe}\frac{\exp(-\lambda_1^2 x/Pe)}{(1+0.02Pe)}. \tag{26a}$$

The factor $(1 + 0.02Pe)$ plays a corrective role since it makes the contribution of axial conduction diminish as *Pe* becomes very large. When $x > 0$, the dash lines in Fig. 8a represent a comparison between the exact series solution and the data from Eq. (26a) with the same $\theta_{b,S}(x)$ as used in Eq. (20a) at very small *x* values. A reasonably good agreement with the exact series solution can facilitate the estimation of total heat flux as *x* goes toward zero. When $x < 0$, a similar estimation for Q_S^* is achieved by integrating Eq. (25) from $-\infty$ and *x*/*Pe* to get

$$-Q_S^*(|x|) = 1 - \theta_{b,S}(x) + \frac{\ln(|x|)}{\pi Pe}\frac{\exp(-\beta_1^2|x|/Pe)}{1+0.02Pe} \tag{26b}$$

with the same functional relation for the contribution of the axial conduction as used in Eq. (26a). The asymptotic $Q_S^*(|x|)$ data using Eq. (26b) are plotted in Fig. 8b and they agree well with the solid lines for the exact solution. The function $\theta_{b,S}(x)$ in Eq. (26a) is the same as that used in Eq. (20b). Also, the Fig. 8b includes the corresponding $Q_L^*(|x|)$ values using the parameters in Table 2b and Eq. (23) after replacing λ_1^2 with β_1^2 and *x* with $|x|$. For large Peclet numbers, it is also possible to get Q^* estimations at large- and small-*x* values by replacing Q_S^* with Q^* and $\theta_{b,S}$ with θ_b as appears in Eqs. (20a,b).

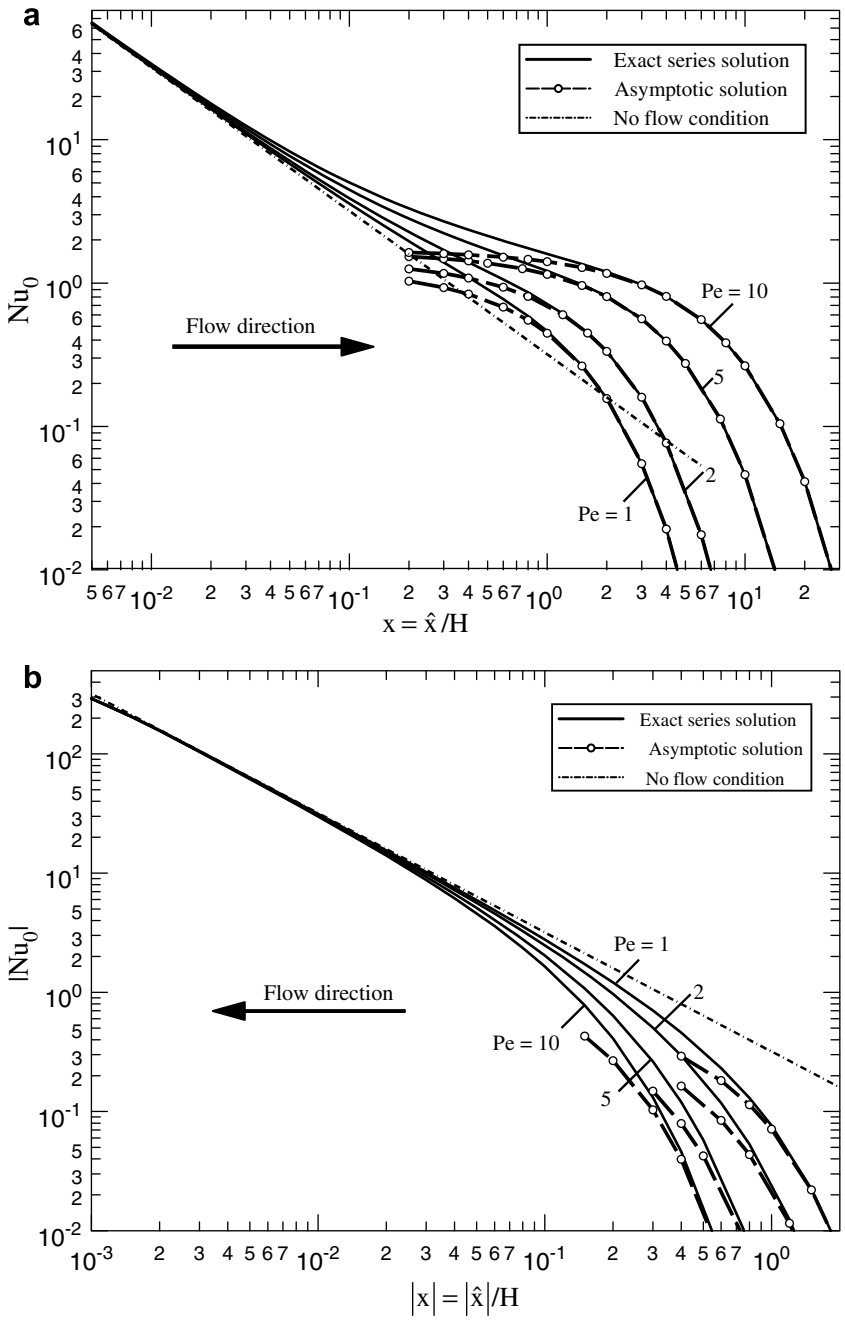

Fig. 7. A comparison of the asymptotic and exact solutions of the Nusselt number for different *Pe* values: as function of $x = \hat{x}/H$ when $x > 0$ and (b) as a function of $|x| = |\hat{x}|/H$ when $x < 0$.

This is because the contribution of axial conduction diminishes as x becomes large when Pe is large, see Table 1 for $Pe = 5$ and 10.

An examination of Eq. (26a) shows that the function $\ln(x)$ slowly goes to infinity as x goes to infinity and, therefore, the exponential terms in Eqs. (26a,b) serve as damping factors. Also, $\ln(x)$ slowly goes to $-\infty$ as x goes toward zero. This increase in the magnitude of Q_S^* toward infinity, as $x \to 0$, is due to the step change in the temperature solution. However, as $x \to 0$, the continuum condition fails and potential remedial steps are discussed in [21]. In practical applications, it is desirable to determine the total wall heat flux between $\hat{x} = 0$ location and a finite $\hat{x} > 0$. To remedy this situation, it is reasonable to hypothesize that $h_0 \approx$ constant within $0 < \hat{x} < \varepsilon$ region when ε is a very small distance, wherein the continuum assumption does not apply. As an example, the wall heat flux between $\hat{x} = 0$ and $\hat{x} > \varepsilon$ is

$$\begin{aligned} Q(0) - Q(\hat{x}) &= \int_0^\infty q_w W \mathrm{d}\hat{x} - \int_{\hat{x}}^\infty q_w W \mathrm{d}\hat{x} \\ &= \int_0^\varepsilon q_w W \mathrm{d}\bar{x} + \int_\varepsilon^\infty q_w W d\hat{x} - \int_{\hat{x}}^\infty q_w W \mathrm{d}\hat{x} \\ &= W\varepsilon h_0(\varepsilon)(T_w - T_i) + Q(\varepsilon) - Q(\hat{x}). \end{aligned} \tag{27}$$

At a predetermined small ε, the heat transfer coefficient relation [21] is $h_0(\varepsilon) = k/(\pi\varepsilon)$ that can also be used to determine ε if the molecular dynamics produces a constant h_0, a priori. Then, Eq. (27) in dimensionless space becomes:

$$Q^*(0) - Q^*(x) = \frac{1}{\pi Pe} + Q^*(\varepsilon/H) - Q^*(x), \tag{28}$$

and for a very small value of ε/H, Eq. (26a) can provide an estimate for $Q^*(\varepsilon/H)$.

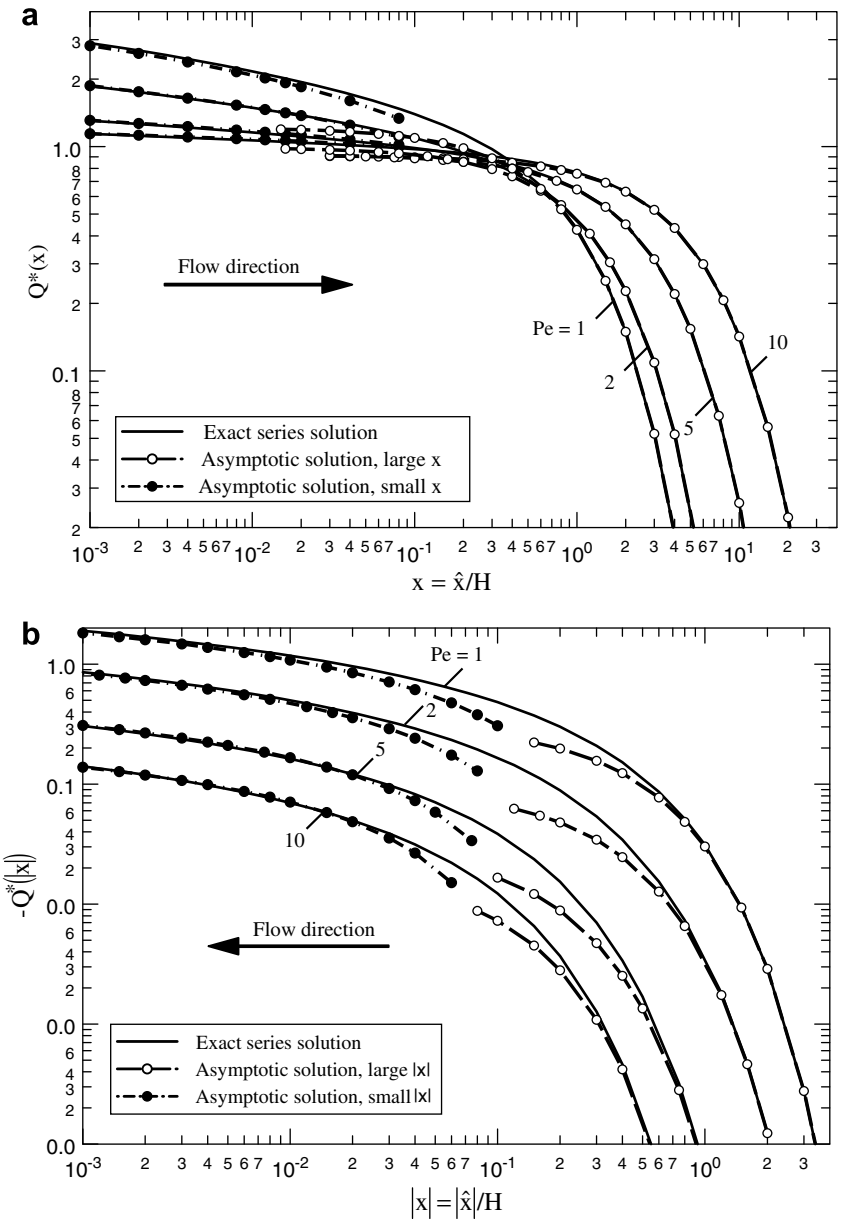

Fig. 8. A comparison of the asymptotic and exact solutions of the total wall heat flux for different *Pe* values: (a) as function of $x = \hat{x}/H$ when $x > 0$ and (b) as a function of $|x| = |\hat{x}|/H$ when $x < 0$.

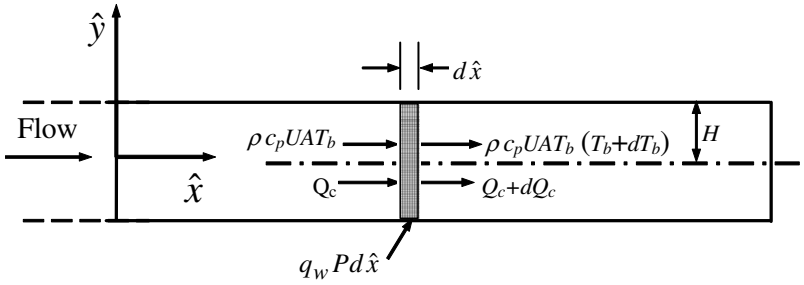

Fig. 9. Energy balance applied to a fluid element with thickness d$\hat{x}$.

Finally, the symbolic software Mathematica [23] was used to acquire the numerical data appearing in this paper. The data appearing in Figs. 4, 5, 7, 8, and 9 are computed with 800 eigenvalues. The parallel plate channels information show the contribution of axial conduction near the thermal entrance location. However, other passages have geometrical differences that can affect the wall heat flux at very small x values. Theoretically, when $\hat{x}$ is smaller than the radius of curvature of the duct, the studies re-

ported in [21] is applicable to other passages, with some modifications. This implies that this solution methodology could be valuable for determining the heat flux at the entrance regions of the ducts with two-dimensional cross sections such as rectangular and triangular ducts. As an example, rectangular passages filled with metallic foams have applications in electronic cooling [6] and the axial conduction should not be ignored, because of the presence of metallic foam.

5. Conclusions

It is shown that the solutions presented at small values of x have relatively small dependency on the size of velocity or the Peclet number. Indeed, both no flow and slip flow conditions provided reasonable limiting values for the Nusselt numbers for all velocity forms between these limiting velocities. Fig. 3 shows that, for $x < 0.01$, the $Nu_0(x)$ solution is the same as that for slug flow over a flat plate and different Pe values have negligible effects. This observation of thermal characteristics at small x values becomes important in the study of heat transfer to fluid within saturated porous passages. The frictional heating effect is ducts deserve a separate study.

Furthermore, the data in Fig. 5 show that neglecting axial conduction can produce relatively large errors. Even for Pe as large as 10, this error could become significant. However, the effect of the axial conduction is small when the Peclet number is well above 10. These approximate values can be useful for estimation of the effects of axial thermal conduction when the actual information is not available. The bulk temperature correlations for these two regions would provide useful information for design applications with reasonable accuracy for the Peclet number above 10, below 1, and in between.

Appendix A. Application of the orthogonality conditions

The orthogonality condition for Eq. (8a) when $\bar{x} < 0$ is

$$\int_0^1 \left[\frac{\beta_m^2+\beta_n^2}{Pe^2} - \frac{u(y)}{U}\right] Y_{1,n}(y)Y_{1,m}(y)\mathrm{d}y = \begin{cases} 0 & \text{when } n \neq m \\ N_m & \text{when } n = m \end{cases}, \tag{A.1a}$$

and for Eq. (8b) when $\bar{x} > 0$ is

$$\int_0^1 \left[\frac{\lambda_m^2+\lambda_n^2}{Pe^2} + \frac{u(y)}{U}\right] Y_{2,n}(y)Y_{2,m}(y)\mathrm{d}y = \begin{cases} 0 & \text{when } n \neq m \\ N_m & \text{when } n = m \end{cases}. \tag{A.1b}$$

Following the related algebraic steps, as given in [12,14], the constants in Eqs. (8a,b) are

$$A_m = \frac{\int_0^1 \left[\frac{\beta_m^2}{Pe^2} - \frac{u(y)}{U}\right] Y_{1,m}(y)\mathrm{d}y}{\int_0^1 \left[\frac{2\beta_m^2}{Pe^2} - \frac{u(y)}{U}\right] Y_{1,m}^2(y)\mathrm{d}y} \quad \text{for } \bar{x} < 0, \tag{A.2a}$$

and

$$B_m = \frac{\int_0^1 \left[\frac{\lambda_m^2}{Pe^2} + \frac{u(y)}{U}\right] Y_{2,m}(y)\mathrm{d}y}{\int_0^1 \left[\frac{2\lambda_m^2}{Pe^2} + \frac{u(y)}{U}\right] Y_{2,m}^2(y)\mathrm{d}y} \quad \text{for } \bar{x} > 0, \tag{A.2b}$$

for $m = 1,2,\ldots$. After further algebraic manipulation, as shown in [12,13], the coefficients A_m and B_m become:

$$A_m = \frac{2}{\beta_m} \frac{1}{[\mathrm{d}Y_{1,m}(y)/\mathrm{d}\beta_m]_{y=1}} \quad \text{for } \bar{x} < 0, \tag{A.3a}$$

$$B_m = -\frac{2}{\lambda_m} \frac{1}{[\mathrm{d}Y_{2,m}(y)/\mathrm{d}\lambda_m]_{y=1}} \quad \text{for } \bar{x} > 0. \tag{A.3b}$$

Note that the parameter A_m depends on the parameters in the θ_1 solution and B_m depends on the parameters in the θ_2 solution; the corresponding eigenvalues λ_m and the eigenfunction $Y_{2,m}(y)$ have values that are different from β_m and $Y_{1,m}(y)$.

As an illustration for $\bar{x} > 0$, following the determination of temperature T and the wall heat flux $q_w = \frac{1}{H}(\partial T/\partial y)|_{y=1}$, the special Nusselt number is obtainable from the relation:

$$Nu_0 = h_0 H/k = -\sum_{m=1}^{\infty} B_m \frac{\mathrm{d}Y_{2,m}(y)}{\mathrm{d}y}\bigg|_{y=1} \mathrm{e}^{-\lambda_m^2 \bar{x}}. \tag{A.4}$$

Also, the dimensionless bulk temperature $\theta_{2,b}$ when $\bar{x} > 0$ is

$$\theta_{2,b} = \frac{T_b - T_w}{T_i - T_w} = \sum_{m=1}^{\infty} B_m \mathrm{e}^{-\lambda_m^2 \bar{x}} \int_0^1 \frac{u(y)}{U} Y_{2,m}(y)\mathrm{d}y$$
$$= \sum_{m=1}^{\infty} B_m \mathrm{e}^{-\lambda_m^2 \bar{x}} \left[-\frac{\lambda_m^2}{Pe^2}\int_0^1 Y_{2,m}(y)\mathrm{d}y - \frac{1}{\lambda_m^2}\frac{\mathrm{d}Y_{2,m}(y)}{\mathrm{d}y}\bigg|_{y=1}\right]. \tag{A.5}$$

Once Nu_0 and θ_b are known, the classical Nusselt number becomes

$$Nu_D = 4h_H/k = \frac{4}{\theta_b} Nu_0 \tag{A.6}$$

Appendix B. Estimation of selected parameters

The bulk temperature at $x = 0$ is the basic and important equation for the determination of heat flow for the wall to the fluid and vice versa. Also for the purpose of verification, the parameter $\theta_b(0)$ was determined from the series solution in both positive x and negative x regions. Its functional values appearing in Tables 2a,b are virtually identical and they attest to the accuracy of series solution. They can also be estimated from the equation:

$$\theta_b = \begin{cases} \frac{0.5+0.239Pe}{1+0.1Pe}, & \text{for } Pe \leqslant 1 \text{ with Error } < 0.3\% \\ \frac{0.95+Pe^{4/3}}{1.9+Pe^{4/3}}, & \text{for } Pe \geqslant 1 \text{ with Error } < 0.5\% \end{cases}. \tag{B.1}$$

The following equations can estimate the parameters λ_1^2, D_1^+, and E_1^+ when $x > 0$ and β_1^2, D_1^-, and E_1^- when $x < 0$. They can provide estimation for these parameters with reasonable accuracy over a broad range of Peclet numbers, in the absence of the actual numerical data. As can be seen from data in Table 2a, $\lambda_1^2 = (\pi/2)Pe$ when Pe approaches 0 and $\lambda_1^2 \cong 1.885$ as Pe becomes very large. These lead to the equations:

$$\lambda_1^2 = \begin{cases} \frac{(\pi/2)Pe}{1+0.45Pe}, & \text{for } Pe \leqslant 0.5, \text{ Error } < 0.35\% \\ \frac{1.887}{\sqrt{1+2.22Pe^{-1.8}}}, & \text{for } Pe \geqslant 0.5, \text{ Error } < 0.4\% \end{cases}. \tag{B.2}$$

Similar relations yield the D_1^+, and E_1^+ parameters:

$$D_1^+ = \begin{cases} \frac{0.4927+0.259Pe^{4/5}}{1+0.2703Pe^{4/5}}, & \text{for } Pe \leqslant 0.2, \text{ Error } < 0.5\% \\ \left(\frac{0.695+0.377Pe^{-1.75}}{1+4.86Pe^{-1.8}}\right)^{1/4}, & \text{for } Pe \geqslant 0.2, \text{ Error } < 0.45\% \end{cases}, \tag{B.3}$$

$$E_1^+ = \begin{cases} \frac{1+0.71Pe}{(1+0.5Pe)^{0.74}}, & \text{for } Pe \leqslant 2, \text{ Error } < 0.6\% \\ \frac{1.713+1.59Pe^{-5/3}}{1+1.63Pe^{-5/3}}, & \text{for } Pe \geqslant 2, \text{ Error } < 0.5\% \end{cases}. \tag{B.4}$$

Similar correlation are prepared for estimation of parameters β_1^2, D_1^-, and E_1^- when $x < 0$; they are

$$\frac{\beta_1^2}{Pe} = \begin{cases} \left(\frac{\pi}{2}\right)(1+0.53Pe), & \text{for } Pe \leqslant 2, \text{ Error } < 3\% \\ \left(\frac{\pi}{2}\right)\left(1+1.4Pe^{0.58}\right) - \frac{4Pe^{0.75}}{(1+0.54Pe)^2}, & \text{for } Pe \geqslant 2, \text{ Error } < 2\% \end{cases}, \tag{B.5}$$

$$D_1^- = \begin{cases} 0.49\exp(-0.451Pe) + \frac{1+0.88Pe^2\exp(-0.2Pe)}{100}, \\ \text{for } Pe \leqslant 5, \text{ Error } < 1.5\% \frac{0.818}{Pe^{0.544}(1+0.495Pe^{0.647})}, , \\ \text{for } Pe \geqslant 5, \text{ Error } < 3\% \end{cases}, \tag{B.6}$$

and

$$E_1^- = \begin{cases} \frac{1}{1+0.5Pe^{5/4}} + \frac{1.34Pe^{7/4}}{(12.4+Pe^{3/2})^{6/5}}, & \text{for } Pe \leqslant 3, \text{ Error } < 2.5\% \\ \frac{0.202Pe^{5/4}}{1+0.102Pe}, & \text{for } Pe \geqslant 3, \text{ Error } < 3.5\% \end{cases}, \quad (B.7)$$

In general, the errors when $x < 0$ is a bit larger than those for $x > 0$ parameters. The main cause is the diminishing the effect of axial conduction in the $x < 0$ region as Pe becomes large.

References

[1] W.M. Kays, M.E. Perkin, Forced convection, internal flow in ducts, section 7, in: W.M. Rohsenow, J.P. Hartnett (Eds.), Handbook of Heat Transfer, McGraw-Hill, New York, 1973.

[2] R.K. Shah, A.L. London, Laminar flow forced convection in ducts, Supplement 1 to Advances in Heat Transfer, Academic Press, New York, 1978.

[3] W.M. Kays, H.C. Crawford, Convective Heat and Mass Transfer, third ed., McGraw-Hill, New York, 1993.

[4] L.C. Burmeister, Convective Heat Transfer, second ed., John Wiley & Sons, New York, 1993.

[5] A. Bejan, Convection Heat Transfer, second ed., John Wiley & Sons, New York, 1982.

[6] D.A. Nield, A. Bejan, Convection in Porous Media, second ed., Springer-Verlog, New York, 1999.

[7] D.A. Nield, A.V. Kuznetsov, M. Xiong, Thermally developing forced convection in a porous medium: parallel-plate channel or circular tube with walls at constant heat flux, J. Porous Media 6 (3) (2003) 203–212.

[8] D.A. Nield, A.V. Kuznetsov, M. Xiong, Thermally developing forced convection in a porous medium: parallel-plate channel or circular tube with isothermal walls, J. Porous Media 7 (1) (2004) 19–27.

[9] A. Haji-Sheikh, K. Vafai, Analysis of flow and heat transfer in porous media imbedded inside various-shaped ducts, Int. J. Heat Mass Transfer 47 (8-9) (2004) 1889–1905.

[10] A. Haji-Sheikh, Estimation of average and local heat transfer in parallel plate and circular ducts filled with porous materials, J. Heat Transfer 126 (3) (2004) 400–409.

[11] A. Haji-Sheikh, W.J. Minkowycz, E.M. Sparrow, A numerical study of the heat transfer to fluid flow through circular porous passages, J. Numer. Heat Transfer 46 (10) (2004) 929–956.

[12] J. Lahjomr, A. Oubarra, Analytical solution of the Graetz problem with axial conduction, ASME J. Heat Transfer 121 (4) (1999) 1078–1083.

[13] J. Lahjomri, A. Oubarra, A. Alemany, Heat transfer by laminar Hartmann flow in thermal entrance region with a step change in wall temperature: the Graetz problem extended, Int. J. Heat Mass Transfer 45 (5) (2002) 1127–1148.

[14] W.J. Minkowycz, A. Haji-Sheikh, Heat transfer in parallel-plate and circular porous passages with axial conduction, Int. J Heat Mass Transfer 49 (13–14) (2006) 2381–2390.

[15] I. Tiselj, G. Hetsroni, B. Mavko, A. Mosyak, E. Pogrebnyak, Z. Segal, Effect of axial conduction on the heat transfer in micro-channels, Int. J. Heat Mass Transfer 47 (12–13) (2004) 2551–2565.

[16] B. Weigand, D. Lauffer, The extended Graetz problem with piecewise constant wall temperature for pipe and channel flows, Int. J. Heat Mass Transfer 47 (22) (2004) 5303–5312.

[17] M.L. Michelsen, J. Villadsen, The Graetz problem with axial heat conduction, Int. J. Heat Mass Transfer 17 (11) (1974) 1391–1402.

[18] D.A. Nield, A.V. Kuznetsov, M. Xiong, Thermally developing forced convection in a porous medium: parallel plate channel with walls at uniform temperature, with axial conduction and viscous dissipation effects, Int. J. Heat Mass Transfer 46 (4) (2003) 643–651.

[19] D.A. Nield, A.V. Kuznetsov, M. Xiong, Thermally developing forced convection in a porous medium: circular ducts with walls at constant temperature, with longitudinal conduction and viscous dissipation effects, Trans. Porous Media 53 (3) (2003) 331–345.

[20] T.V. Nguyen, Laminar heat transfer for thermally developing flow in ducts, Int. J. Heat Mass Transfer 35 (7) (1992) 1733–1741.

[21] A. Haji-Sheikh, D.E. Amos, J.V. Beck, Axial heat conduction in a moving semi-infinite fluid, Int. J. Heat Mass Transfer 51 (19-20) (2008) 4651–4658.

[22] A. Haji-Sheikh, J.V. Beck, Entrance effect on heat transfer to laminar flow through passages, Int. J. Heat Mass Transfer 50 (17) (2007) 3340–3350.

[23] S. Wolfram, The Mathematica Book, fifth ed., Cambridge University press, Cambridge, UK, 2005.